Enhanced glucose-induced intracellular signaling promotes insulin hypersecretion: pancreatic beta-cell functional adaptations in a model of genetic obesity and prediabetes.

Running title: Increased beta-cell function in ob/ob mice

Esperanza Irles[1,2], Patricia Ñeco[1,2], Mónica Lluesma[1,2], Sabrina Villar-Pazos[1,2], Junia Carolina Santos-Silva[1,3], Jean F. Vettorazzi[1,3], Paloma Alonso-Magdalena[1,2], Everardo M. Carneiro[3], Antonio C. Boschero[3], Ángel Nadal[1,2], Ivan Quesada[1,2,*]

[1] *Instituto de Bioingeniería, Universidad Miguel Hernández, Elche, Spain.*

[2] *CIBER de Diabetes y Enfermedades Metabólicas Asociadas (CIBERDEM), Spain.*

[3] *Department of Structural and Functional Biology, Institute of Biology, State University of Campinas (UNICAMP), Campinas, Brazil.*

*to whom reprint requests should be addressed:

I. Quesada. Instituto de Bioingeniería, Universidad Miguel Hernández, Avenida de la Universidad s/n, 03202 Elche, Spain. Phone: (+34) 96 522 2003. Email: ivanq@umh.es

Keywords: pancreatic beta-cell, diabetes, obesity, calcium signals, electrical activity, insulin secretion.

ABSTRACT

Obesity is associated with insulin resistance and is known to be a risk factor for type-2 diabetes. In obese individuals, pancreatic beta-cells try to compensate for the increased insulin demand in order to maintain euglycemia. Most studies have reported that this adaptation is due to morphological changes. However, the involvement of beta-cell functional adaptations in this process needs to be clarified. For this purpose, we evaluated different key steps in the glucose-stimulated insulin secretion (GSIS) in intact islets from female *ob/ob* obese mice and lean controls. Obese mice showed increased body weight, insulin resistance, hyperinsulinemia, glucose intolerance and fed hyperglycemia. Islets from *ob/ob* mice exhibited increased glucose-induced mitochondrial activity, reflected by enhanced NAD(P)H production and mitochondrial membrane potential hyperpolarization. Perforated patch-clamp examination of beta-cells within intact islets revealed several alterations in the electrical activity such as increased firing frequency and higher sensitivity to low glucose concentrations. A higher intracellular Ca^{2+} mobilization in response to glucose was also found in *ob/ob* islets. Additionally, they displayed a change in the oscillatory pattern and Ca^{2+} signals at low glucose levels. Capacitance experiments in intact islets revealed increased exocytosis in individual *ob/ob* beta-cells. All these up-regulated processes led to increased GSIS. In contrast, we found a lack of beta-cell Ca^{2+} signal coupling, which could be a manifestation of early defects that lead to beta-cell malfunction in the progression to diabetes. These findings indicate that beta-cells functional adaptations are an important process in the compensatory response to obesity.

1. Introduction.

Obese individuals are at increased risk for type 2 diabetes. Hyperinsulinemia along with low insulin sensitivity are frequently observed in obesity (Kahn et al., 2006). Although insulin resistance is present in most obese subjects, glucose intolerance and hyperglycemia are not necessarily found in these individuals. Indeed, compensatory adaptations in the pancreatic β-cells usually allow for higher pancreatic insulin release in order to maintain normoglycemic values (Kargar and Ktorza, 2008; Seino et al., 2011). However, when β-cell compensations fail to adapt to the increasing insulin requirements imposed by insulin resistance, glucose tolerance becomes deteriorated in obese individuals and, eventually, they can develop overt hyperglycemia and type-2 diabetes (Kahn et al., 2006). Several studies in animal models and humans have reported that the enhanced plasma insulin levels observed in insulin-resistant states, like in obesity, are likely related with increases in β-cell mass (Sachdeva and Stoffers, 2009; Seino et al., 2011; Saisho et al., 2013). In contrast, other studies in non-diabetic obese human subjects have shown that beta-cell mass was only moderately increased (Rahier et al., 2008) compared with controls or that there were no differences (Kou et al., 2013). However, less importance has been attributed to the involvement of the β-cell function in these compensatory responses (Hull et al., 2005). Consequently, changes in the β-cell stimulus-secretion coupling remain poorly characterized in obesity (Kargar and Ktorza, 2008; Seino et al., 2011).

Recently, our group reported that β-cells from high fat diet-induced obese mice display several functional adaptations. In this insulin-resistant state, β-cell compensations led to insulin hypersecretion, maintaining normal glycemia and glucose tolerance in obese mice (Gonzalez et al., 2013). However, in the progression from normoglycemia to overt diabetes, insufficient β-cell compensation to insulin resistance

can result in a prediabetic condition characterized by impaired glucose tolerance and moderate hyperglycemia (Weir and Bonner-Weir, 2004). In order to analyze this prediabetic state, here we aimed to elucidate the functional changes in the β-cell glucose-stimulated insulin secretion (GSIS) using a model of genetic obesity. The leptin-deficient *ob/ob* mouse is characterized by marked obesity, insulin resistance, glucose intolerance, moderate hyperglycemia and elevated plasma insulin levels, but they do not develop overt type 2 diabetes (Coleman, 1978). Given that *ob/ob* mice have larger islets of Langerhans (Bleisch et al., 1952; Gepts et al., 1960; Bock et al., 2003) with a higher proportion of β-cells (Baetens et al., 1978; Gepts et al., 1960; Westman, 1968a; Westman, 1968b), they have been extensively used as a source of pancreatic islets. Although numerous investigations have used *ob/ob* islets for β-cell studies (Hellman, 1965; Hellman, 1970; Bergsten et al., 1994), a detailed analysis of the potential functional adaptations in the different steps of the stimulus-secretion coupling is still lacking. Additionally, most data about the islet function comes from isolated β-cells (Ahmed and Grapengiesser, 2001; Grapengiesser et al., 1988), an experimental model that can differ from the physiological scenario, as it has been reported using intact islets (Göpel et al., 1999; Göpel et al., 2000; Göpel et al., 2004). In the current study, we show in intact pancreatic *ob/ob* islets that improved performance in the majority of steps involved in GSIS would account for the high insulin secretion rate characteristic of hyperinsulinemic insulin-resistant conditions, like in obesity. Additionally, the present findings further support the wide plasticity and crucial adaptation of the β-cell secretory process in the compensatory responses of the endocrine pancreas.

2. Material and Methods

2.1. Animals. All protocols were approved by our Animal Ethics Committee according to national regulations. Five-week-old female *ob/ob* mice (C57BL/6J background) were purchased from Harlan Laboratories (Barcelona, Spain) and lean female of matched age were used as controls. In electrophysiological experiments, *ob/ob* female animals (C57BL/6J background) were purchased from Janvier (Janvier Labs, Le Genest sur l'Isle, France). Animals were housed at 22ºC with a light cycle of 12 hours (8:00 am to 8:00 pm) and had free access to water and standard chow. Experiments were performed when animals were 12 weeks old.

2.2. Plasma measurements and tolerance tests. Glucose and insulin plasma levels were measured by tail bleeding in fed state and during tolerance tests (Gonzalez et al., 2013). Plasma glucose was measured with a commercial glucometer (Accu-Chek) and plasma insulin by a commercial ELISA kit (Crystal Chemical). For the glucose tolerance test, animals were fasted for 12 hours before an intraperitoneal (i.p.) glucose injection (2g/kg). Plasma glucose was measured at 0, 15, 30, 60, 90, 120 and 180 min and plasma insulin at 0 and 30 min after the glucose challenge. For the insulin tolerance test, fed animals were subjected to an i.p. insulin injection (1UI/kg) and then, plasma glucose was measured at 0, 15, 30, 45 y 60 min. The HOMA-IR was also calculated as an indicator of insulin resistance: [fasted plasma glucose (mg/dL) * fasted plasma insulin (mU/L)] / 405 (Tripathy et al., 2010; Solomon et al., 2014).

2.3. Islet isolation and cell culture. Mice were sacrificed at the age of 12 weeks by cervical dislocation. Islets were isolated by collagenase digestion as previously described (Gonzalez et al., 2013). In some experiments, islets were subjected to trypsin digestion to obtain isolated cells, and then cultured overnight at 37ºC in RPMI 1640

98 (Sigma, Madrid, Spain) supplemented with 10% fetal bovine serum, 100 IU/mL
99 penicillin, 0.1 mg/mL streptomycin and 11mM D-glucose (Quesada et al., 2000).
100 **2.4. Patch-clamp recordings.** Electrophysiological measurements were performed
101 from superficial β-cells in intact islets using an EPC-10 USB patch-clamp amplifier and
102 the Patch Master Software suite (HEKA Elektronic, Lambrecht/Pfatz, Germany). Intact
103 islets were hold by gentle suction applied to the interior of a wide-bore holding pipette
104 as previously reported (Göpel et al., 1999). The perforated-patch configuration was used
105 for the membrane potential recordings (Gonzalez et al., 2013). The pipette solution
106 contained (in mM): 76 K_2SO_4, 10 NaCl, 10 KCl, 1 $MgCl_2$, 5 HEPES (pH=7.35 with
107 KOH), and 0.24 mg/mL of the pore-forming antibiotic amphotericin B; the bath
108 solution contained (in mM): 140 NaCl, 3.6 KCl, 1.5 $CaCl_2$, 5 $NaHCO_3$, 0.5 $MgSO_4$, 0.5
109 NaH_2PO_4, 10 HEPES (pH=7.4 with NaOH) and D-glucose as indicated. Exocytosis was
110 monitored using the standard whole-cell configuration and recording cell capacitance
111 changes through the sine +DC mode of the Lock-In amplifier included in the Patch
112 Master software (Gonzalez et al., 2013). For these experiments, the pipette solution
113 contained (in mM): 140 CsCl, 10 NaCl, 1 $MgCl_2$, 0.05 EGTA, 3 Mg-ATP, 0.1 cAMP
114 and 5 HEPES (pH=7.2 with CsOH), whereas the bath solution contained (in mM): 118
115 NaCl, 5.6 KCl, 20 tetraethylammonium-Cl, 1.2 $MgCl_2$, 5 $CaCl_2$, 5 HEPES and 5 D-
116 glucose (pH=7.4 with NaOH). Only experiments with stable and low access resistance
117 and small leak currents were used. The seal resistance was typically >3 MΩ. All
118 experiments were carried out at physiological temperature (34-36ºC). β-cells were
119 functionally identified by the ability to generate the characteristic oscillatory electrical
120 activity in the presence of glucose and steady-state inactivation of Na^+ currents (Göpel
121 et al., 1999; Göpel et al., 2000; Gonzalez et al. 2013).

2.5. Intracellular Ca^{2+}, NAD(P)H and mitochondrial membrane potential measurements. Isolated islets were allowed to recover in the isolation medium for at least 2 hours at 37ºC and 5% CO_2 before experiments. For intracellular calcium ($[Ca^{2+}]_i$) recordings, islets were incubated for 1h at room temperature with 2μM fura-2 (for conventional fluorescence microscopy) or fluo-4 (for confocal microscopy). For intact islet Ca^{2+} signaling, recordings were performed under an inverted epifluorescence microscope (Axiovert 200; Zeiss, Jena, Germany) equipped with 360 and 380nm band-pass filters. Recordings were expressed as the ratio of fluorescence at 360 and 380 (F360/380). Images were taken every 3 seconds. Intracellular $[Ca^{2+}]$ changes in response to stimuli were analyzed as previously described (Rafacho et al., 2010). For transient changes in $[Ca^{2+}]_i$, the basal fluorescence (F_0) was subtracted to the maximal fluorescence and expressed as ΔF ($F-F_0$). Additionally, as a measure of global $[Ca^{2+}]_i$ increase, the area under the curve (AUC) was calculated on the last five minutes of each glucose stimulus. Changes in NAD(P)H autofluorescence and mitochondrial membrane potential ($\Delta\Psi_m$) were monitored with the above-mentioned imaging system (Rafacho et al., 2010). For NAD(P)H autofluorescence, a 365nm band-pass filter was used, and emission was filtered at 445±25 nm. Images were acquired every 60 seconds. For measurement of NAD(P)H in isolated cells, cells were cultured overnight in RPMI 1640. Recordings were plotted as the increase of fluorescence referred to the fluorescence in the basal condition. $\Delta\Psi_m$ was measured after loading fresh isolated islets for 10 minutes with 10μM rhodamine-123 (Rhod-123). Images were taken every 30 seconds using conventional fluorescein filters. Recordings were plotted as the decrease of fluorescence relative to the fluorescence in the basal condition. For the analysis of β-cell synchrony, whole islets were used to monitor changes in $[Ca^{2+}]_i$

within individual cells using a confocal microscope (Zeiss LSM510 laser), as previously reported (Gonzalez et al., 2013; Quesada et al., 2006).

2.6. Insulin secretion and content. Isolated islets recovered in the isolation medium for 2h in the incubator (37ºC; 5% CO_2). After recovery, batches of 5 islets were exposed to the different glucose stimuli and allowed to secrete for 1h at 37ºC (solution composition in mM: 140 NaCl, 4.5 KCl, 2.5 $CaCl_2$, 1 $MgCl_2$, 20 HEPES, pH=7.4). The totality of the secretion volume (500µL) was collected and then measured by RIA, in duplicate, using a Coat-a-Count kit (Siemens, Los Angeles, California). The groups of 5 islets were transferred to an ethanol/HCl buffer to promote cell lysis. After overnight incubation at 4ºC, the supernatant was used to quantify insulin content by RIA and total protein by the Bradford method. Insulin secretion was expressed normalized either by insulin content or total protein, as previously shown (Gonzalez et al., 2013).

2.7. Quantitative real-time PCR. Total RNA from islets of Langerhans was isolated using the RNeasy Plus Mini Kit (Qiagen) and the RNA concentration was determined by spectrophotometry (NanoDrop 2000, Thermo Scientific). cDNA was synthesized from 500ng of total RNA using the High Capacity cDNA Reverse Transcription Kit (Applied Biosystems). Quantitative PCR reactions were performed using the CFX96 Real Time System (Bio-Rad, Hercules, California). Reactions were carried out in a final volume of 10µL, containing 200nM of each primer, 1µL of cDNA and 1X of iQ™ SYBR®Green supermix (Bio-Rad). Samples were subjected to the following thermal cycler conditions: 10min at 95ºC, 45 cycles (10s at 95ºC, 7s at 60ºC, 15s at 72ºC) and melting curve from 65 to 95ºC with a slope of 0.1ºC/s. The gene for relative quantification was *GAPDH*. The resulting values were analyzed with CFX Manager version 1.6 (Bio-Rad) and values were expressed as the relative expression respect to control levels ($2^{-\Delta\Delta Ct}$). Primer sequences are described in Supplemental Table 1.

2.8. Western blot. Groups of 200-300 islets were subjected to lysis in 20µL of Cell Lysis Buffer (Cell Signaling Technology, Danvers, MA). For SDS gel electrophoresis and Western blot analysis, samples were treated with a Laemmli sample buffer containing dithiothreitol. After heating at 95ºC for 5 minutes, proteins were separated by electrophoresis in a 4-20% Mini Protean Gel (Bio Rad). Prestained SDS-PAGE standards were included for molecular mass estimation. Transfer to PVDF membranes was performed in a Trans Blot Turbo transfer for 7 minutes in 25V, with TRIS/Glycine buffer (Bio Rad). After membranes were blocked with 5% non-fat dry milk buffer, they were incubated with a polyclonal antibody against Connexin36 (1:1000; Invitrogen) or β-Tubulin (1:1000; Cell Signaling). Visualization of specific protein bands was performed by incubating the membranes with appropriate secondary antibodies. Protein bands were revealed by using the Chemi Doc MP System (Bio Rad). The band intensities were quantified with the Image Lab Lale 4.1 TM Software (Bio Rad).

2.9. Measurement of islet size. The pancreas was extracted and fixed in 4% paraformaldehyde. The tissue was then processed and embedded in paraffin and sections were prepared. Staining was performed as previously described (Gonzalez et al., 2013). The area of pancreatic islets was analyzed using the Metamorph Software (Molecular Devices, Sunnyvale, CA).

2.10. Data analysis. Data are shown as mean ± SE unless otherwise stated. Statistical comparisons between groups were performed using the unpaired Student's *t*-test, with Welch's correction when mandatory. Differences were considered significant when $p < 0.05$.

3. Results.

3.1. Metabolic features in *ob/ob* mice related with glucose homeostasis. Twelve-week old *ob/ob* mice displayed an increased body weight that was twice that of age-matched CTL (controls; Fig. 1A) (40.82 ± 0.43 g vs 20.77 ± 0.15 g, respectively). Obese mice exhibited increased plasma glucose concentrations in the fed state (Fig. 1B), despite the high levels of fed plasma insulin compared with controls (Fig. 1C). Additionally, o*b/ob* mice were insulin resistant (Fig. 1D; Supplemental Fig. 1) and glucose intolerant (Fig. 1E). The glucose tolerance test (Fig. 1E, F) showed that fasting plasma glucose tended to be higher in o*b/ob* mice (although not statistically significant), and that these obese animals displayed glucose intolerance, as evidenced by the high plasma glucose levels maintained over the 3 hours subsequent to the glucose challenge. In the control group, plasma glucose clearance reached basal levels after 90-120 min, whereas in the obese group plasma glucose remained elevated even after 180 min. Finally, after an i.p. glucose load, plasma insulin levels were found higher at 0 and 30 min in *ob/ob* mice (Fig. 1G, H). Altogether, these results indicate that, although *ob/ob* mice exhibit higher insulin responses to glucose changes, this adaptation would not fully compensate the requirements imposed by insulin resistance to maintain normoglycemia. Thus, since *ob/ob* mice represent a good model to study this prediabetic state characterized by insulin resistance and glucose intolerance, we aimed to study the different steps involved in GSIS.

3.2. Enhanced mitochondrial function in *ob/ob* islets. Glucose metabolism yields redox power by means of nicotinamide adenine dinucleotide (NADH) and flavin adenine dinucleotide ($FADH_2$) production (Quesada et al., 2006). This reducing power, mainly produced by the tricarboxylic acid cycle in the mitochondria, is used as a source for electron transfer in the oxidative phosphorylation required to produce ATP (Quesada

et al., 2006; Rafacho et al., 2010). In an attempt to monitor changes in the mitochondrial redox state induced by glucose metabolism, we performed NAD(P)H autofluorescence experiments in CTL and *ob/ob* intact islets. As shown in Figure 2A, increasing glucose concentrations produced gradual increments in NAD(P)H fluorescence in both groups. Interestingly, *ob/ob* islets showed an enhanced NAD(P)H production at each glucose concentration tested (Fig. 2B). When the data was normalized to calculate the glucose concentration required to reach the half maximal fluorescence, we found that the glucose dose-response curve was shifted to lower glucose concentrations in *ob/ob* islets (CTL: 8.77mM G; *ob/ob*: 6.77mM G) (Fig. 2C). To further confirm the increased mitochondrial activity in islets from obese mice, we monitored changes in the mitochondrial membrane potential (ψ_m), as this parameter depends on glucose metabolism. Increasing glucose concentrations lead to ψ_m hyperpolarization (Rafacho et al., 2010). To monitor ψ_m, we loaded islets with the lipophylic fluorescent dye rhodamine-123 (Rhod-123), which intercalates into the mitochondrial membranes in a potential-dependent manner. Figure 2D shows the typical gradual decrease in Rhod-123 fluorescence, when glucose concentrations were stepwise increased. In agreement with the results obtained with NAD(P)H fluorescence, *ob/ob* islets exhibited a higher ψ_m hyperpolarization at all the glucose concentrations (Fig. 2D and E). When Rhod-123 fluorescence was normalized in both groups to obtain the glucose concentration associated to the half maximal fluorescence, we did not get differences between both groups (Fig. 2F). This might probably due to the lower sensitivity of this experiment to produce glucose-mediated fluorescence compared with the NAD(P)H assays (Fig. 2A, D). Consistent with the rest of results, we also found enhanced NAD(P)H production in isolated β-cells from *ob/ob* mice (Fig. 2G, H). This improved glucose-induced mitochondrial response in *ob/ob* islets might not be associated with up-regulation of

early metabolic steps, since we found decreased glucose transporter-2 expression in *ob/ob* islets (~68% decrease vs CTL) and comparable levels of glucokinase gene expression in both groups (Supplemental Fig. 2).

3.3. Obese mice display several alterations in the membrane potential of β-cells. The following experiments were performed using perforated-patch recordings in β-cells within intact islets to preserve the cell-to-cell environment, which is more similar to the physiological scenario (Göpel et al., 1999; Göpel et al., 2000; Göpel et al., 2004). Compared with the characteristic membrane potential oscillations in response to 11 mM glucose in controls (Fig. 3A), *ob/ob* β-cells displayed a different profile (Fig. 3B). In *ob/ob*, the firing frequency of the action potentials was slightly increased (Fig. 3C), in combination with a much longer duration of the burst (Fig. 3D) and longer silent phases between bursts (Fig. 3E). Interestingly, a more detailed analysis of the membrane potential recordings (Fig. 3F,G) showed that the burst was initiated at less negative potentials in β-cells from obese mice (CTL, -71.7 ± 1.9 mV; *ob/ob*, -57.2 ± 2.7 mV) (Fig. 3H). Furthermore, the action potentials of *ob/ob* β-cells started at a more depolarized potential (CTL, -47,5 ± 2,2 mV; *ob/ob*, -39,8 ± 1,8 mV) (Fig. 3I) and peaks reached less negative potentials (CTL, -24,1 ± 2,9 mV; *ob/ob*, -12,1 ± 2,2 mV) (Fig. 3J). As we will discuss later, this different electrical activity in *ob/ob* mice, particularly the higher frequency and burst duration, should have an impact on Ca^{2+} signaling, since action potentials in mouse β-cells are mainly mediated by Ca^{2+} channels (Göpel et al., 1999; Rorsman and Braun, 2013).

3.4. Islets from obese mice exhibit enhanced glucose-induced Ca^{2+} signals. Ca^{2+} signaling plays a key role in coupling glucose metabolism and insulin release. As a next step in the β-cell stimulus-secretion process, we analyzed intracellular Ca^{2+} signals in whole islets, as previously described (Rafacho et al., 2010; Gonzalez et al., 2013).

While *ob/ob* islets displayed an enlarged Ca^{2+} signal in response to 5.6 and 8 mM glucose compared with controls, no differences were found at 16 mM, when the AUC was calculated as a measure of the global Ca^{2+} entry (Fig. 4A-C). This analysis evidenced that the Ca^{2+} signal in *ob/ob* islets at 5.6 mM glucose was of the same magnitude than that of CTL islets at 8mM glucose. A similar equivalence was observed between the intracellular Ca^{2+} in *ob/ob* islets at 8mM glucose and CTL islets at 16mM glucose (Fig. 4C). When we analyzed the fluorescence increase (ΔF) of the first Ca^{2+} transient at each glucose stimulus, differences were only found at 5.6mM glucose (Fig. 4D). This was related to the fact that the totality of *ob/ob* islets displayed Ca^{2+} signaling at this glucose concentration, whereas in most of the CTL islets any Ca^{2+} entry was detected (Fig. 4E). The oscillatory pattern was also modified in islets from obese mice. While CTL islets showed the characteristic pattern with oscillations of high frequency after the first transient at 8mM glucose, *ob/ob* islets showed lower frequency Ca^{2+} signals (Fig. 4F). We next analyzed the response to a stimulus independent of metabolism. Exposure to 75mM KCl led to a depolarization-induced Ca^{2+} transient (Fig. 4G). The amplitude of this transient was not different between both groups (Fig. 4H), suggesting that increased Ca^{2+} signaling in obese mice were due to changes in glucose metabolism. The non-glucidic fuel alpha-ketoisocaproate (KIC) has been shown to produce Ca^{2+} oscillations in pancreatic islets (Martin et al., 1995). KIC also led to enhanced Ca^{2+} signaling in islets from obese mice compared with lean controls (Supplemental Fig. 3), further suggesting that metabolism is particularly affected in ob/ob animals. In summary, glucose-regulated Ca^{2+} signaling in *ob/ob* islets was mainly characterized by higher magnitude and higher sensitivity to glucose compared with controls.

3.5. Insulin secretion and exocytosis are increased in *ob/ob* pancreatic islets. Insulin gene expression (Fig. 5A) as well as insulin content (Fig. 5B) were found to be increased in *ob/ob* islets as compared to CTL. As previously documented (Black et al., 1986; Fournier et al., 1990), we observed that insulin secretion was enhanced in islets from obese mice (Supplemental Fig. 4). Since it has been reported that the exocytotic process measured in isolated β-cells largely differs from that measured in islets (Göpel et al., 2004), we studied exocytosis in β-cells within the pancreatic islets, which better resembles the physiological cell-to-cell interactions. When we analyzed capacitance changes in response to depolarization pulses, we found that exocytosis in *ob/ob* β-cells was higher than in CTL cells (Fig. 5C, D), indicating that enhanced insulin secretion in intact islets is also due to augmented exocytosis at the single cell level.

3.6. β-cell coupling is altered in the islets of obese mice. Analysis of intracellular Ca^{2+} signals in individual β-cells within the pancreatic islets, as reported previously (Gonzalez et al. 2013), showed that cell-to-cell coupling was reduced in *ob/ob* β-cells compared with controls (Fig. 6A, B). When the lag time was calculated between the first and the last beta-cell responding with a Ca^{2+} increase to 11 mM glucose within a single islet, we observed that the average time was 58.04 ± 9.14 seconds in *ob/ob* islets and 4.68 ± 1.34 seconds in CTL islets (Fig. 6C), indicating a lower synchrony in the former group. While *connexin36* mRNA levels were similar in both groups, the protein content was significantly reduced in *ob/ob* islets (Supplemental Fig. 5). Gap junctions in the mouse β-cell are mainly composed by Cx36. Additionally, we found that *ob/ob* β-cells responded 1.35 ± 0.15 min faster to 11 mM glucose than control cells (Fig.6D), which is consistent with the higher glucose sensitivity observed in the previous experiments (Fig. 2,4).

Discussion.

During obesity, the endocrine pancreas undergoes several adaptations to compensate for the insulin resistance characteristic of this state. Structural adaptations, by means of an increment in the β-cell mass, have been extensively reviewed in both animals and humans (Butler et al., 2003; Sachdeva et al., 2009; Seino et al., 2011; Saisho et al. 2013). In agreement with previous reports in ob/ob mice (Bock et al., 2003), we also found increased islet size (Supplemental Fig. 6). However, less is known about the β-cell functional adaptations (Kahn et al., 2006; Kargar and Ktorza, 2008; Seino et al., 2011). We have previously demonstrated in a model of high fat diet-induced obesity that pancreatic β-cells exhibit an improved function in several events involved in GSIS (Gonzalez et al., 2013). These adaptations allowed for a compensation of insulin resistance, preserving normoglycemia and glucose tolerance in this model. It has been proposed that, in the progression from this normoglycemic state to overt diabetes in obese subjects, compensatory adaptations become insufficient to counteract insulin resistance, leading to an intermediate state characterized by hyperinsulinemia, moderate hyperglycemia and glucose intolerance (Weir and Bonner-Weir, 2004). However, there is no information about this prediabetic condition at the functional level. In the present study, we have taken advantage of the *ob/ob* mouse metabolic characteristics, which resemble this prediabetic state, to explore the β-cell function. At the age of 12 weeks, *ob/ob* mice exhibited glucose intolerance and insulin resistance, in agreement with previous publications (Saleh et al., 2006). Despite the high circulating insulin levels, obese mice were only able to maintain plasma glucose levels within the normoglycemic range in the fasted state but not during fed conditions or during an i.p. glucose challenge (Fig. 1). Although the hyperinsulinemic characteristic of *ob/ob* mice has been related with morphological adaptations (Tomita et al., 1992; Baetens et al.,

1978; Gepts et al., 1960), increased GSIS has been also observed in isolated ob/ob islets (Black et al., 1986; Fournier et al., 1990. Saleh et al., 2006). In the present work, we focused on the involvement of the different functional steps participating in GSIS.

In β-cells, most of the NAD(P)H synthesis derived from glucose metabolism takes place in the mitochondria (Patterson et al., 2000). We showed here an enhanced NAD(P)H production and glucose sensitivity in islets of obese mice (Fig. 2). This effect was also observed in individual β-cells, which supports that the enhanced NAD(P)H signal found in intact islets would not be due to increased β-cell number but a consequence of metabolic adaptations in individual β-cells. Additionally, *ob/ob* islets displayed higher glucose-induced ψ_m hyperpolarization, further supporting an enhanced β-cell mitochondrial performance in obese mice. All these findings are in agreement with previous reports showing similar metabolic responses in a rat model of insulin resistance (Rafacho et al., 2010). Since enhanced NAD(P)H production and Ψ_m hyperpolarization should be coupled to increased ATP synthesis (Quesada et al., 2006), the mitochondrial responses in *ob/ob* islets and their higher glucose sensitivity may explain the electrical activity at lower glucose levels compared with controls (Fig. 3). Likewise, since β-cell Ca^{2+} signaling is mediated by electrical activity, the intracellular Ca^{2+} entry observed at 5.6 mM glucose in *ob/ob* islets (Fig. 4) would be also associated with the improved mitochondrial activity. In addition to electrical and Ca^{2+} signaling effects, it has been shown that ATP and other glucose-stimulated mitochondrial factors like glutamate and, particularly, NAD(P)H can also exert a positive regulation of exocytosis and secretory granules mobilization (Maechler and Wollheim, 1999; Ivarsson et al., 2005; Reinbothe et al., 2009; MacDonald, 2011; Rorsman and Braun, 2013). Thus, all these cellular events are expected to be augmented in *ob/ob* β-cells. Furthermore, we found reduced *GLUT2* expression in *ob/ob* islets, while *GcK*

367 expression was not altered (Supplemental Fig. 2). Despite the decreased *GLUT2*
368 expression, which has also been reported at the protein level in *ob/ob* islets (Jetton et al,
369 2001), glucose metabolism is not necessarily affected by this alteration, since the
370 limiting enzyme in the glycolytic pathway is GcK (Chen et al., 1994). Thus, the
371 enhanced mitochondrial activity shown in *ob/ob* β-cells might result from alterations
372 other than in these proteins.

373 It has been previously reported that glucose usage is mainly glycolytic in the
374 pancreatic beta-cell and that glucose-induced NAD(P)H fluorescence comes
375 fundamentally from mitochondria rather than from cytosol in the pancreatic islet
376 (Patterson et al., 2000; Quesada et al., 2006). Thus, this protocol allows for the temporal
377 analysis of mitochondrial activity. Our results indicate a left-shift displacement in the
378 dose-response curve of the glucose-induced NAD(P)H fluorescence (Fig. 2C),
379 indicating a higher sensitivity for low and intermediate glucose levels in obese animals,
380 as previously indicated (Chen et al., 1993). A similar finding was found in glucose-
381 induced Ca^{2+} signals (Fig. 4). The NAD(P)H results are in agreement with previous
382 findings showing increased ATP production at low glucose concentrations in islets of
383 ob/ob mice compared with lean controls, while no significant differences were observed
384 at high glucose levels (Saleh et al., 2006). In this study, it was also reported that ob/ob
385 islets express more uncoupling protein-2 (UCP2) than controls, which may contribute to
386 GSIS impairment (Saleh et al., 2006). Given that UCP2 activation is associated with Ψ_m
387 dissipation (Fink et al., 2002), our experiments (Fig. 2D-F) argue against a negative
388 impact of this protein on beta-cell Ψ_m in ob/ob mice.

389 β-cells from *ob/ob* mice display an electrical activity pattern that differs from
390 that of controls, as it has been previously reported (Rosario et al., 1985). Among other
391 features, this electrical pattern is characterized by a higher sensitivity to low glucose

concentrations. This hyper-excitability has been related to altered K^+ permeabilities (Fournier et al., 1990; Rosario, 1985). These observations would be in accordance with the lower density of K_{ATP} channels in the membrane of β-cells from *ob/ob* mice (Park et al., 2013). Alternatively, here we show that the improved glucose-induced electrical activity in *ob/ob* islets may be also explained by their enhanced mitochondrial activity at lower glucose concentrations (Fig. 2), in agreement with previous works (Saleh et al., 2006). Additionally, in line with other studies (Rosario et al., 1985), the firing frequency and the duration of the electrical activity bursts were increased in obese mice (Fig. 3). Both characteristics would be associated with the higher Ca^{2+} signals observed in *ob/ob* islets (Fig. 4), given that action potentials in mouse β-cells result from Ca^{2+} channel activity, which lead to Ca^{2+} entry (MacDonald, 2011). Moreover, the burst and action potential baseline were slightly depolarized compared with controls (Fig. 4), which may suggest an altered activity of Ca^{2+}-activated K^+ channels, as previously indicated (Rosario et al., 1985; Rosario, 1985; Black et al., 1988). It has been reported that higher action potentials may be associated to increased inward Ca^{2+} currents due to the voltage-dependence characteristics of Ca^{2+} channels (Gonzalez et al., 2013; Houamed et al., 2010; Jacobson et al., 2010). Thus, it is possible that the higher peak level of the ob/ob action potentials (Fig. 3J) may also contribute to the increased Ca^{2+} signals shown here (Fig. 4).

Ca^{2+} signals in response to 5.6 and 8mM glucose were enhanced in islets from *ob/ob* mice (Fig. 4). Other studies have not reported differences, probably because *ob/ob* islets were stimulated by glucose concentrations (20 mM) at which β-cells were maximally depolarized (Fournier et al., 1993). In contrast to the glucose effects, no differences were found by KCl stimulation, which further supports the idea that increased Ca^{2+} signals in *ob/ob* islets may be mediated by changes in glucose

417 metabolism or metabolic-related factors (Ivarsson et al., 2005; MacDonald, 2011;
418 Rorsman and Braun, 2013), particularly at low-intermediate glucose levels. The idea
419 that metabolism could be affected in ob/ob islets was also supported by the higher
420 response to KIC. As we have mentioned above, the enhanced Ca^{2+} signals would be also
421 related to the higher action potential frequency and longer burst duration characteristic
422 of *ob/ob* beta-cells. Additionally, most *ob/ob* islets displayed a different oscillatory
423 pattern, characterized by the loss of high frequency oscillations (Fig. 4). This has been
424 attributed to a reduced expression of the TRPM5 channel (Colsoul et al., 2010; Colsoul
425 et al., 2013). Our findings in *TRPM5* gene expression agree with this effect on the Ca^{2+}
426 oscillatory frequency (Supplemental Fig. 2). This channel is a non-selective monovalent
427 cation channel activated by intracellular Ca^{2+} that contributes to membrane
428 depolarization during electrically silent intervals, promoting the initiation of a new burst
429 activity. This would also explain the absence of fast membrane potential oscillations in
430 *ob/ob* (Fig. 3), as described for *Trpm5*$^{-/-}$ islets (Colsoul et al., 2010). However, Colsoul
431 *et al*. found no differences between controls and *Trpm5*$^{-/-}$ islets in the glucose
432 concentration threshold that trigger $[Ca^{2+}]_i$ oscillations. In *ob/ob* islets, this might be
433 explained by the lower K_{ATP} density in the plasma membrane (Park et al., 2013) and an
434 enhanced glucose metabolism, as we showed here.

435 The increased insulin secretory capacity in *ob/ob* islets has been reported long
436 time ago (Black et al., 1986; Fournier et al., 1990). Our capacitance experiments in
437 intact islets demonstrate that this hypersecretion may be supported by an enhanced
438 exoytotic capacity at the single cell level. Additionally, given that capacitance changes
439 were elicited by depolarization pulses (instead of glucose stimuli), it also indicates that
440 the exocytotic process *per se* is subjected to an adaptive process in *ob/ob* β-cells
441 independent of glucose metabolism that would increase the secretory process. In any

442 case, since it has been reported that NAD(P)H can directly affect β-cell exocytosis
443 (Ivarsson et al., 2005; Reinbothe et al., 2009), the increased NAD(P)H responses
444 reported here might be also involved in the augmented exocytosis in *ob/ob* β-cells. In
445 line with other reports (Saleh et al., 2006), we also observed enhanced insulin secretion
446 at low glucose concentrations in ob/ob islets (Supplemental Fig. 4), although no
447 differences were found in Ca^{2+} levels. This augmented basal secretion may be due to
448 up-regulated constitutive insulin secretion or that beta-cell secretory granules contain
449 more insulin compared with controls. However, much research would be necessary to
450 explore these possibilities. It has been proposed that GSIS is modulated by both
451 triggering and metabolic amplifying pathways (Henquin, 2009), that are mainly relayed
452 by Ca^{2+} and metabolic factors, respectively. Although we did not perform specific
453 experiments in the current study to understand the potential contribution of each
454 pathway in the augmented GSIS in ob/ob islets, several findings such as the elevated
455 Ca^{2+} levels and mitochondrial function suggest that both pathways might be involved.

456 Cell-to-cell coupling among β-cells allows electrical and Ca^{2+} signaling
457 synchrony within the islet (Nadal et al., 1999; Quesada et al., 2006). This coupling is
458 necessary to maintain a proper insulin secretion and alterations in this coordination are
459 detrimental for this process (Vozzi et al., 1995; Charollais et al., 2000). We observed
460 decreased Ca^{2+} signal coupling among β-cells of *ob/ob* islets in agreement with previous
461 studies (Ravier et al., 2002). C*onnexin36*, which is the main connexin type expressed in
462 mouse islets, was reduced at the protein level in ob/ob islets compared with controls.
463 Thus, this protein reduction may contribute to the deficient coupling observed in obese
464 islets. Additionally, given that electrical and Ca^{2+} signal transmission within the islet
465 decay with the intercellular distance (Andreu et al., 1997; Quesada et al., 2003), it is
466 plausible that the decreased coupling in *ob/ob* islets are also associated with their larger

size compared with controls (Gepts et al., 1960; Baetens et al., 1978; Tomita et al., 1992), as it has been previously suggested (Ravier et al., 2002). This possibility would require further investigation. Thus, among the different events studied in the present work, Ca^{2+} signal coupling was the only one to be decreased. Since we have previously observed normal coupling in islets of obese normoglycemic mice (Gonzalez et al., 2013), it is tempting to speculate that this could be an early defect in the prediabetic state that takes place in the progression to diabetes in obese individuals.

In summary, while the islet compensatory response to obesity and insulin resistant states has been mainly related to morphological changes, here we show that β-cell functional adaptations have also a key role in this process. Additionally, we also demonstrated that almost all the events implicated in GSIS are augmented in magnitude and/or glucose sensitivity, indicating a significant plasticity in β-cell function in non-physiological and pathological conditions. Finally, we also detected a lack of β-cell coordination in obese prediabetic mice that could be an early manifestation of functional defects that lead to GSIS failure and diabetes. All these adaptations may offer a broad spectrum of possibilities for the design of therapeutic approaches that may slow down the progression to diabetic states in obese individuals.

Acknowledgements. We thank M. S. Ramon and M. L. Navarro for their expert technical assistance. This work was supported by grants from the Spanish Ministerio de Ciencia e Innovación (BFU2013-42789-P; BFU2011-28358), Generalitat Valenciana (PROMETEO/2011/080), and the European Foundation for the Study Diabetes (EFSD/BI Basic Programme). CIBERDEM is an initiative of the Instituto de Salud Carlos III.

Disclosure Summary: The authors have nothing to disclose.

References

Ahmed, M., Grapengiesser, E., 2001. Pancreatic beta-cells from obese-hyperglycemic mice are characterized by excessive firing of cytoplasmic Ca2+ transients. Endocrine. 15(1):73-8.

Andreu, E., Soria, B., Sanchez-Andres, J.V., 1997. Oscillation of gap junction electrical coupling in the mouse pancreatic islets of Langerhans. J Physiol. 498 (Pt 3):753-61.

Baetens, D., Stefan, Y., Ravazzola, M., Malaisse-Lagae, F., Coleman, D.L., Orci, L., 1978. Alteration of islet cell populations in spontaneously diabetic mice. Diabetes. 27(1):1-7.

Bergsten, P., Grapengiesser, E., Gylfe, E., Tengholm, A., Hellman, B., 1994. Synchronous oscillations of cytoplasmic Ca2+ and insulin release in glucose-stimulated pancreatic islets. J Biol Chem. 269(12):8749-53.

Black, M.A., Fournier, L.A., Heick, H.M., Bégin-Heick, N., 1988. Different insulin-secretory responses to calcium-channel blockers in islets of lean and obese (ob/ob) mice. Biochem J. 249(2):401-7.

Black, M., Heick, H.M., Bégin-Heick, N., 1986. Abnormal regulation of insulin secretion in the genetically obese (ob/ob) mouse. Biochem J. 238(3):863-9.

Bleisch, V.R., Mayer, J., Dickie, M.M., 1952. Familial diabetes mellitus in mice, associated with insulin resistance, obesity, and hyperplasia of the islands of langerhans. Am J Pathol. 28(3):369-85.

Bock, T., Pakkenberg, B., Buschard, K., 2003. Increased islet volume but unchanged islet number in ob/ob mice. Diabetes 52:1716–22.

Butler, A.E., Janson, J., Soeller, W.C., Butler, P.C., 2003. Increased beta-cell apoptosis prevents adaptive increase in beta-cell mass in mouse model of type 2 diabetes: evidence for role of islet amyloid formation rather than direct action of amyloid. Diabetes. 52(9):2304-14.

Charollais, A., Gjinovci, A., Huarte, J., Bauquis, J., Nadal, A., Martín, F., et al., 2000. Junctional communication of pancreatic beta cells contributes to the control of insulin secretion and glucose tolerance. J Clin Invest. 106(2):235-43.

Chen, C., Hosokawa, H., Bumbalo, L.M., Leahy, J.L., 1994. Mechanism of compensatory hyperinsulinemia in normoglycemic insulin-resistant spontaneously hypertensive rats. Augmented enzymatic activity of glucokinase in beta-cells. J Clin Invest. 94(1):399-404.

Chen, N.G., Tassava, T.M., Romsos, D.R., 1993. Threshold for glucose-stimulated insulin secretion in pancreatic islets of genetically obese (ob/ob) mice is abnormally low. J Nutr. 123(9):1567-1574.

Coleman, D.L., 1978. Obese and diabetes: two mutant genes causing diabetes-obesity syndromes in mice. Diabetologia. 14(3):141-8.

Colsoul, B., Jacobs, G., Philippaert, K., Owsianik, G., Segal, A., Nilius, B., et al., 2014. Insulin downregulates the expression of the Ca2+-activated nonselective cation channel TRPM5 in pancreatic islets from leptin-deficient mouse models. Pflugers Arch. 466(3):611-21.

Colsoul, B., Schraenen, A., Lemaire, K., Quintens, R., Van Lommel, L., Segal, A., et al., 2010. Loss of high-frequency glucose-induced Ca2+ oscillations in pancreatic islets correlates with impaired glucose tolerance in Trpm5-/- mice. Proc Natl Acad Sci U S A. 107(11):5208-13.

Fink, B.D., Hong, Y.S., Mathahs, M.M., Scholz, T.D., Dillon, J.S., Sivitz, W.I., 2002. UCP2-dependent proton leak in isolated mammalian mitochondria. J Biol Chem. 277(6):3918-25.

Fournier, L., Whitfield, J.F., Xiang, H., Schwartz, J.L., Bégin-Heick, N., 1993. K+ channel and alpha 2-adrenergic effects on glucose-induced Ca2+i surges: aberrant behavior in ob/ob mice. Am J Physiol. 264(6 Pt 1):C1458-65.

Fournier, L.A., Heick, H.M., Bégin-Heick, N., 1990. The influence of K(+)-induced membrane depolarization on insulin secretion in islets of lean and obese (ob/ob) mice. Biochem Cell Biol. 68(1):243-8.

Gepts, W., Christophe, J., Mayer, J., 1960. Pancreatic islets in mice with the obese-hyperglycemic syndrome: lack of effect of carbutamide. Diabetes. 9:63-9.

Gonzalez, A., Merino, B., Marroquí, L., Ñeco, P., Alonso-Magdalena, P., Caballero-Garrido, E., et al., 2013. Insulin hypersecretion in islets from diet-induced hyperinsulinemic obese female mice is associated with several functional adaptations in individual β-cells. Endocrinology. 154(10):3515-24.

Göpel, S., Kanno, T., Barg, S., Galvanovskis, J., Rorsman, P., 1999. Voltage-gated and resting membrane currents recorded from B-cells in intact mouse pancreatic islets. J Physiol. 15;521 Pt 3:717-28.

Göpel, S., Zhang, Q., Eliasson, L., Ma, X.S., Galvanovskis, J., Kanno, T., et al., 2004. Capacitance measurements of exocytosis in mouse pancreatic alpha-, beta- and delta-cells within intact islets of Langerhans. J Physiol. 556(Pt 3):711-26.

Göpel, S.O., Kanno, T., Barg, S., Rorsman, P., 2000. Patch-clamp characterisation of somatostatin-secreting -cells in intact mouse pancreatic islets. J Physiol. 528(Pt 3):497-507.

Grapengiesser, E., Gylfe, E., Hellman, B., 1988. Glucose-induced oscillations of cytoplasmic Ca2+ in the pancreatic beta-cell. Biochem Biophys Res Commun. 151(3):1299-304.

Hellman, B., 1965. Studies in obese-hyperglycemic mice. Ann N Y Acad Sci. 1965 Oct 8;131(1):541-58.

Hellman, B., 1970. Methodological approaches to studies on the pancreatic islets. Diabetologia. 1970 Apr;6(2):110-20.

Henquin, J.C., 2009. Regulation of insulin secretion: a matter of phase control and amplitude modulation. Diabetologia. 52(5):739-751.

Houamed, K.M., Sweet, I.R., Satin, L.S., 2010. BK channels mediate a novel ionic mechanism that regulates glucose-dependent electrical activity and insulin secretion in mouse pancreatic beta-cells. J Physiol 588:3511-3523.

Hull, R.L., Kodama, K., Utzschneider, K.M., Carr, D.B., Prigeon, R.L., Kahn SE., 2005. Dietary-fat-induced obesity in mice results in beta cell hyperplasia but not increased insulin release: evidence for specificity of impaired beta cell adaptation. Diabetologia. 48(7):1350-8.

Ivarsson, R., Quintens, R., Dejonghe, S., Tsukamoto, K., in 't Veld, P., Renström, E., et al., 2005. Redox control of exocytosis: regulatory role of NADPH, thioredoxin, and glutaredoxin. Diabetes. 54(7):2132-42.

Jacobson, D.A., Mendez, F., Thompson, M., Torres, J., Cochet, O., Philipson, L.H., 2010. Calcium-activated and voltage-gated potassium channels of the pancreatic islet impart distinct and complementary roles during secretagogue induced electrical responses. J Physiol 588:3525-3537.

Jetton, T.L., Liang, Y., Cincotta, A.H., 2001. Systemic treatment with sympatholytic dopamine agonists improves aberrant beta-cell hyperplasia and GLUT2, glucokinase, and insulin immunoreactive levels in ob/ob mice. Metabolism. 50(11):1377-84.

Kahn, S.E., Hull, R.L., Utzschneider, K.M., 2006. Mechanisms linking obesity to insulin resistance and type 2 diabetes. Nature 444:840-846.

595 Kargar, C., Ktorza, A., 2008. Anatomical versus functional beta-cell mass in
596 experimental diabetes. Diabetes Obes Metab. 10 Suppl 4:43-53.
597 Kou, K., Saisho, Y., Satoh, S., Yamada, T., Itoh, H., 2013. Change in β-cell mass in
598 Japanese nondiabetic obese individuals. J Clin Endocrinol Metab. 98(9):3724-3730.
599 MacDonald, P.E., 2011. Signal integration at the level of ion channel and exocytotic
600 function in pancreatic β-cells. Am J Physiol Endocrinol Metab. 301(6):E1065-9.
601 Maechler, P., Wollheim, C.B., 1999. Mitochondrial glutamate acts as a messenger in
602 glucose-induced insulin exocytosis. Nature. 402(6762):685-9.
603 Martin, F., Sanchez-Andres, J.V., Soria, B., 1995. Slow [Ca2+]i oscillations induced by
604 ketoisocaproate in single mouse pancreatic islets. Diabetes. 44(3):300-5.
605 Nadal, A., Quesada, I., Soria, B., 1999. Homologous and heterologous asynchronicity
606 between identified alpha-, beta- and delta-cells within intact islets of Langerhans in
607 the mouse. J Physiol. 517 (Pt 1):85-93.
608 Park, S.H., Ryu, S.Y., Yu, W.J., Han, Y.E., Ji, Y.S., Oh, K., Sohn, J.W., et al., 2013.
609 Leptin promotes K(ATP) channel trafficking by AMPK signaling in pancreatic β-
610 cells. Proc Natl Acad Sci U S A. 110(31):12673-8.
611 Patterson, G.H., Knobel, S.M., Arkhammar, P., Thastrup, O., Piston, D.W., 2000.
612 Separation of the glucose-stimulated cytoplasmic and mitochondrial NAD(P)H
613 responses in pancreatic islet beta cells. Proc Natl Acad Sci U S A. 97(10):5203-7.
614 Quesada, I., Fuentes, E., Andreu, E., Meda, P., Nadal, A., Soria, B., 2003. On-line
615 analysis of gap junctions reveals more efficient electrical than dye coupling
616 between islet cells. Am J Physiol Endocrinol Metab. 284(5):E980-7.
617 Quesada, I., Martín, F., Soria, B., 2000. Nutrient modulation of polarized and sustained
618 submembrane Ca2+ microgradients in mouse pancreatic islet cells. J Physiol. 525
619 Pt 1:159-67.
620 Quesada, I., Todorova, M.G., Alonso-Magdalena, P., Beltrá, M., Carneiro, E.M.,
621 Martin, F., ET al., 2006. Glucose induces opposite intracellular Ca2+ concentration
622 oscillatory patterns in identified alpha- and beta-cells within intact human islets of
623 Langerhans. Diabetes. 55(9):2463-9.
624 Quesada, I., Todorova, M.G., Soria, B., 2006. Different metabolic responses in alpha-,
625 beta-, and delta-cells of the islet of Langerhans monitored by redox confocal
626 microscopy. Biophys J. 90(7):2641-50.
627 Rafacho, A., Marroquí, L., Taboga, S.R., Abrantes, J.L., Silveira, L.R., Boschero, A.C.,
628 et al., 2010. Glucocorticoids in vivo induce both insulin hypersecretion and
629 enhanced glucose sensitivity of stimulus-secretion coupling in isolated rat islets.
630 Endocrinology. 151(1):85-95.
631 Rahier, J., Guiot, Y., Goebbels, R.M., Sempoux, C., Henquin, J.C., 2008. Pancreatic
632 beta-cell mass in European subjects with type 2 diabetes. Diabetes Obes Metab. 10
633 Suppl 4:32-42.
634 Ravier, M.A., Sehlin, J., Henquin, J.C., 2002. Disorganization of cytoplasmic Ca(2+)
635 oscillations and pulsatile insulin secretion in islets from ob/ob mice. Diabetologia.
636 45(8):1154-63.
637 Reinbothe, T.M., Ivarsson, R., Li, D.Q., Niazi, O., Jing, X., Zhang, E., Stenson, L.,
638 Bryborn, U., Renström., E., 2009. Glutaredoxin-1 mediates NADPH-dependent
639 stimulation of calcium-dependent insulin secretion. Mol Endocrinol. 23(6):893-
640 900.
641 Rorsman, P., Braun, M., 2013. Regulation of insulin secretion in human pancreatic
642 islets. Annu Rev Physiol. 75:155-79.

643 Rosario, L.M., Atwater, I., Rojas, E., 1985. Membrane potential measurements in islets
644 of Langerhans from ob/ob obese mice suggest an alteration in [Ca2+]i-activated K+
645 permeability. Q J Exp Physiol. 70(1):137-50.
646 Rosario, L.M., 1985. Differential effects of the K+ channel blockers apamin and quinine
647 on glucose-induced electrical activity in pancreatic beta-cells from a strain of ob/ob
648 (obese) mice. FEBS Lett. 188(2):302-6.
649 Sachdeva, M.M., Stoffers, D.A., 2009. Minireview: Meeting the demand for insulin:
650 molecular mechanisms of adaptive postnatal beta-cell mass expansion. Mol
651 Endocrinol. 23(6):747-58.
652 Saisho, Y., Butler, A.E., Manesso, E., Elashoff, D., Rizza, R.A., Butler, P.C., 2013. β-
653 cell mass and turnover in humans: effects of obesity and aging. Diabetes Care. 2013
654 36(1):111-7.
655 Saleh, M.C., Wheeler, M.B., Chan, C.B., 2006. Endogenous islet uncoupling protein-2
656 expression and loss of glucose homeostasis in ob/ob mice. J Endocrinol.
657 190(3):659-67.
658 Seino, S., Shibasaki, T., Minami, K., 2011. Dynamics of insulin secretion and the
659 clinical implications for obesity and diabetes. J Clin Invest. 121(6):2118-25.
660 Solomon, G., Atkins, A., Shahar, R., Gertler, A., Monsonego-Ornan. E, 2014. Effect of
661 peripherally administered leptin antagonist on whole body metabolism and bone
662 microarchitecture and biomechanical properties in the mouse. Am J Physiol
663 Endocrinol Metab. 306(1):E14-27.
664 Tripathy, S., Torres-Gonzalez, M., Jump, D.B., 2010. Elevated hepatic fatty acid
665 elongase-5 activity corrects dietary fat-induced hyperglycemia in obese C57BL/6J
666 mice. J Lipid Res. 51(9):2642-54.
667 Tomita, T., Doull, V., Pollock, H.G., Krizsan, D., 1992. Pancreatic islets of obese
668 hyperglycemic mice (ob/ob). Pancreas. 7(3):367-75.
669 Vozzi, C., Ullrich, S., Charollais, A., Philippe, J., Orci, L., Meda, P., 1995. Adequate
670 connexin-mediated coupling is required for proper insulin production. J Cell Biol.
671 131(6 Pt 1):1561-72.
672 Weir, G.C., Bonner-Weir, S., 2004. Five stages of evolving beta-cell dysfunction during
673 progression to diabetes. Diabetes. 53 Suppl 3:S16-21.
674 Westman, S., 1968a. The endocrine pancreas of old obesehyperglycemic mice. Acta Soc
675 Med Ups. 73(1):81-9.
676 Westman, S., 1968b. Development of the obese-hyperglycaemic syndrome in mice.
677 Diabetologia. 4(3):141-9.
678

FIGURE LEGENDS.

Figure 1. Metabolic features in control and *ob/ob* mice. A, Body weight (n=35 and n=28 for control and *ob/ob* mice, respectively). B, Plasma glucose in the fed state in CTL (n=26) and *ob/ob* mice (n=23). C, Plasma insulin in the fed state in CTL (n=13) and *ob/ob* mice (n=11). D, Insulin resistance calculated by HOMA-IR in CTL (n=8) and *ob/ob* mice (n=6). E, Glucose tolerance test (n=8 for CTL and n=7 for *ob/ob* mice). F, Area under the curve from experiment in E. G and H, Plasma glucose (G) and insulin (H) measured in CTL (n=8) and *ob/ob* (n=6) just before an i.p. glucose load and 30 min after. Statistical significance is indicated: *, $p \leq 0.05$; **, $p \leq 0.01$; ***, $p \leq 0.001$; ns, non-significant.

Figure 2. NAD(P)H generation and mitochondrial membrane potential ($\Delta\psi_m$) changes in intact control and *ob/ob* islets. A, Changes in NAD(P)H autofluorescence at increasing glucose concentrations (percentage referred to the signal in the basal condition: 0.5mM glucose). The trace represents the average of 6 different experiments per group. B, The graph represents the mean ± SEM of the maximal NAD(P)H autofluorescence values at the end of each glucose stimulus shown in A. C, Mean ± SEM of the maximal NAD(P)H autofluorescence values at each glucose concentration, normalized in each group from 0 to 100%. The value of the glucose concentration to reach half the maximal fluorescence in each group is indicated in the graph. D, Changes in Rhod123 fluorescence at increasing glucose concentrations. The trace represents the average of 8 and 9 different experiments in CTL and *ob/ob*, respectively. E, Mean ± SEM of the minimal Rhod123 fluorescence values at the end of each glucose stimulus. F, Mean ± SEM of the minimal Rhod123 fluorescence values at each glucose concentration, normalized in each group from 0 to 100%. G, Changes in NAD(P)H autofluorescence at increasing glucose concentrations in CTL (n=20) and *ob/ob* (n=66)

isolated cells. H, Mean ± SEM of the maximal NAD(P)H autofluorescence values at the end of each glucose stimulus from experiment in G. Statistical significance is indicated: *, p≤0.05; **, p≤0.01; ***, p≤0.001; ns, non-significant.

Figure 3. Electrical activity in control and *ob/ob* β-cells. A and B, Representative examples of membrane potential changes in response to 11mM glucose in CTL (A; n=6) and *ob/ob* (B; n=6) β-cells. Recordings were performed in beta-cells within intact islets. C, D and E, Firing frequency (C), burst duration (D) and interburst duration (E) from experiments shown in A and B. F and G, Detail of figures A and B, respectively, at expanded temporal scale. H, I, J, Burst baseline (H), action potential baseline (I) and mean peak voltage of the action potentials (J) from recordings shown in F and G (n=5 for CTL and n=6 for *ob/ob*). Statistical significance is indicated: *, p≤0.05; **, p≤0.01.

Figure 4. Glucose-induced Ca^{2+} signaling in β-cells of control and *ob/ob* mice. A, Representative intracellular Ca^{2+} signals measured in intact CTL (n=8) and *ob/ob* (n=6) islets by fluorescence microscopy and fura-2 in response to 8mM and 16mM glucose. B, Representative intracellular Ca^{2+} signals measured in intact CTL (n=9) and *ob/ob* (n=8) islets in response to 5.6mM and 8mM glucose. C, Analysis of the area under the curve on the last five minutes of each glucose stimulus from experiments shown in A and B. D, Analysis of the fluorescence increase (ΔF) of the first Ca^{2+} transient in response to each glucose challenge from experiments shown in A and B. E, Percentage of responsive islets to 5.6mM glucose (n=9 for CTL; n=8 for *ob/ob*). All the islets from both groups responded to 8 and 16mM glucose. F, Oscillations per minute in CTL and ob/ob islets at 8 and 16mM glucose. G, Representative intracellular Ca^{2+} signals in response to depolarization induced by a short pulse of KCl (75mM; n=10 for CTL; n=6 for *ob/ob*). H, Analysis of the fluorescence increases (ΔF) shown in G. Statistical significance is indicated: *, p≤0.05; **, p≤0.01; ***, p≤0.001; ns, non-significant.

730 **Figure 5. Insulin secretion and exocytosis.** A, Insulin gene expression in islets from
731 CTL and *ob/*ob (n=5). B, Insulin content normalized to total protein in CTL (n=16) and
732 *ob/ob* (n=15) islets. C, Representative capacitance responses to ten 500-millisecond
733 depolarizing pulses (from -70 to 0 mV) in CTL and *ob/ob* β-cells. Recordings were
734 performed in beta-cells within intact islets. D, Membrane capacitance at the end of the
735 depolarizing protocol normalized by cell size (n=10 for CTL; n=45 for *ob/ob*).
736 Statistical significance is indicated: *, $p \leq 0.05$; **, $p \leq 0.01$; ***, $p \leq 0.001$; ns, non-
737 significant.

738 **Figure 6**. **β-cell coupling in *ob/ob* islets.** A and B, Representative Ca^{2+} signals in
739 several individual β-cells within a CTL (A) or an ob/ob islet (B). C, Mean time delay
740 between the first cell that responds to 11 mM glucose and the rest of β-cells within an
741 islet was calculated to measure the degree of Ca^{2+} signaling synchrony. In each
742 experimental group, the time at which the first cell responded to high glucose was set as
743 t=0, and then, the delay of the response of the rest of cells of the same islet was
744 determined. D, Temporal delays in the β-cell Ca^{2+} response to glucose. The mean time
745 of the response to 11 mM glucose in CTL β-cells was set as t=0, and then, the
746 anticipation or delay of the response of *ob/ob* β-cells was calculated. Statistical
747 significance is indicated: ***, $p \leq 0.001$.

Figure 1.

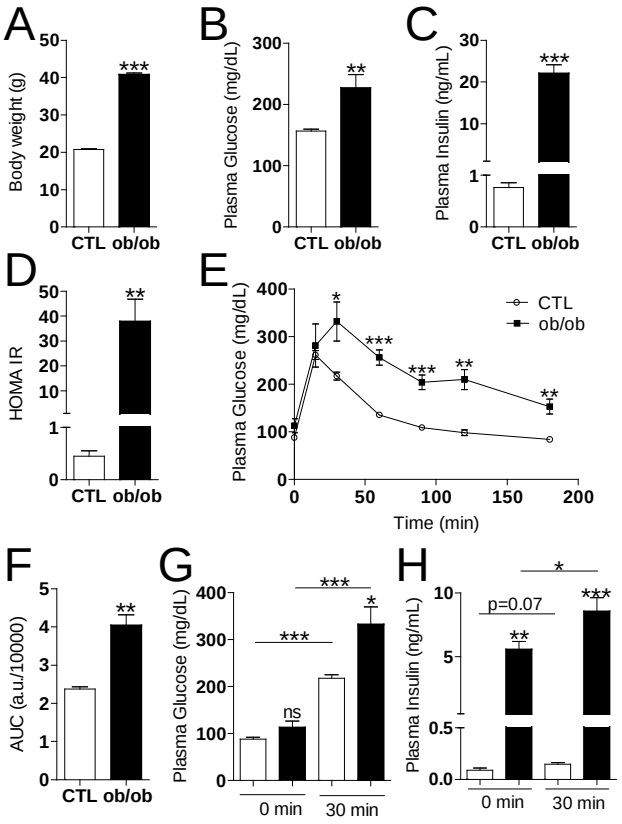
A
Body weight (g)
50
40
30
20
10
0
***
CTL ob/ob
B
Plasma Glucose (mg/dL)
300
200
100
0
**
CTL ob/ob
C
Plasma Insulin (ng/mL)
30
20
10
1
0
***
CTL ob/ob
D
HOMA IR
50
40
30
20
10
1
0
**
CTL ob/ob
E
Plasma Glucose (mg/dL)
400
300
200
100
0
CTL
ob/ob
*
***
***
**
**
0
50
100
150
200
Time (min)
F
AUC (a.u./10000)
5
4
3
2
1
0
**
CTL ob/ob
G
Plasma Glucose (mg/dL)
400
300
200
100
0
***
***
*
ns
0 min
30 min
H
Plasma Insulin (ng/mL)
10
5
0.5
0.0
p=0.07
**
*
***
0 min
30 min

Figure 2.

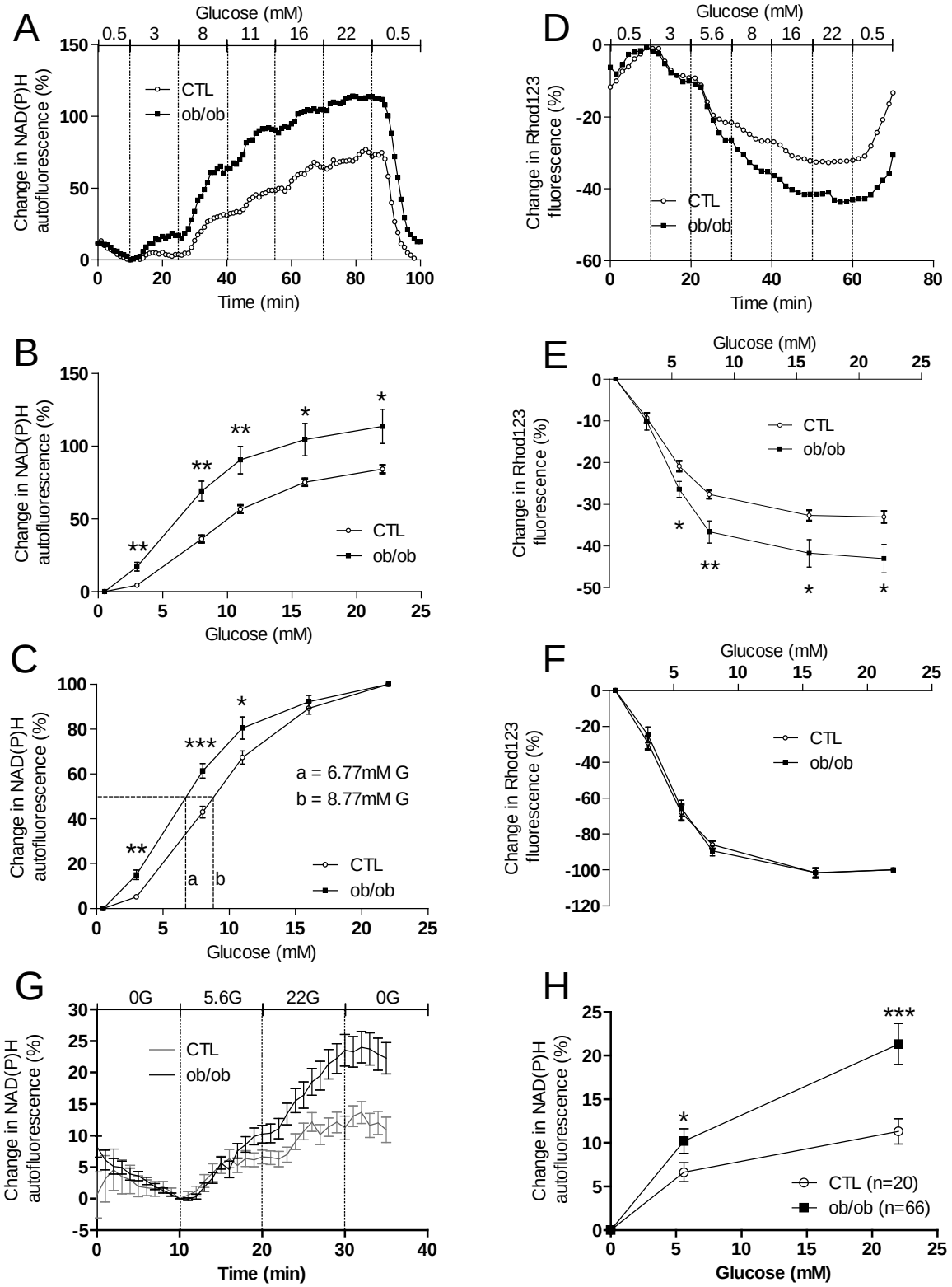
A
Glucose (mM)
0.5 3 8 11 16 22 0.5
Change in NAD(P)H autofluorescence (%)
CTL
ob/ob
Time (min)
B
Change in NAD(P)H autofluorescence (%)
CTL
ob/ob
Glucose (mM)
C
Change in NAD(P)H autofluorescence (%)
a = 6.77mM G
b = 8.77mM G
a
b
CTL
ob/ob
Glucose (mM)
D
Glucose (mM)
0.5 3 5.6 8 16 22 0.5
Change in Rhod123 fluorescence (%)
CTL
ob/ob
Time (min)
E
Glucose (mM)
Change in Rhod123 fluorescence (%)
CTL
ob/ob
F
Glucose (mM)
Change in Rhod123 fluorescence (%)
CTL
ob/ob
G
0G 5.6G 22G 0G
Change in NAD(P)H autofluorescence (%)
CTL
ob/ob
Time (min)
H
Change in NAD(P)H autofluorescence (%)
CTL (n=20)
ob/ob (n=66)
Glucose (mM)

Figure 3.

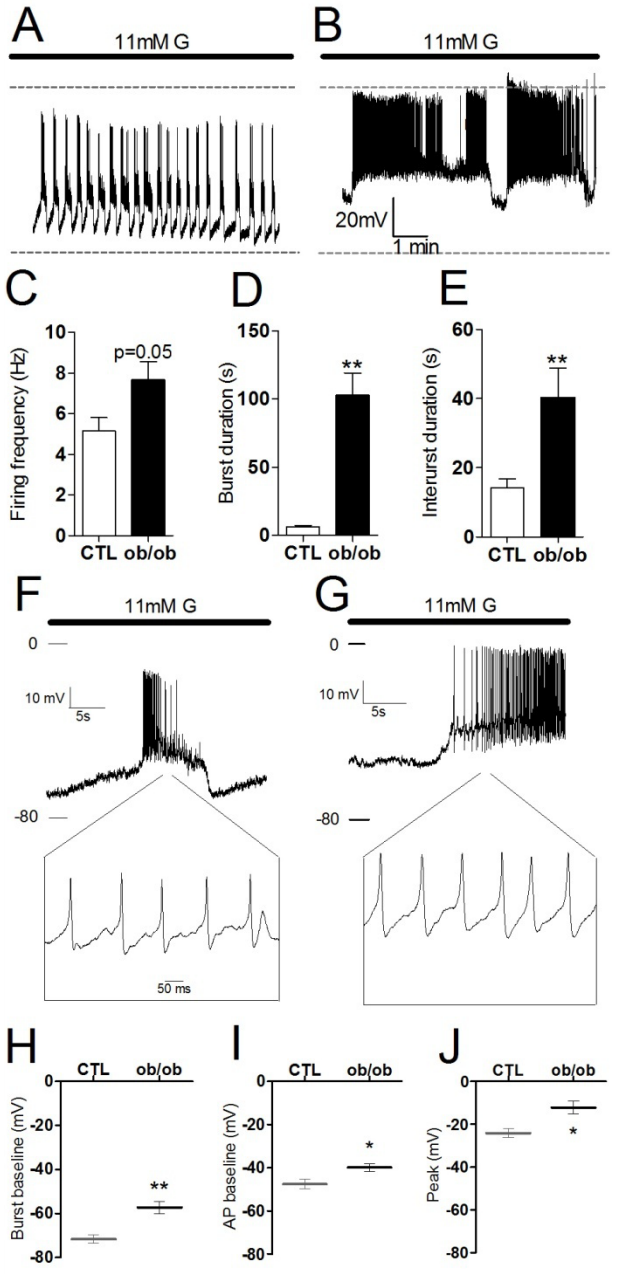
A
11mM G
B
11mM G
20mV
1 min
C
Firing frequency (Hz)
p=0.05
CTL ob/ob
D
Burst duration (s)
**
CTL ob/ob
E
Interurst duration (s)
**
CTL ob/ob
F
11mM G
0
10 mV
5s
-80
50 ms
G
11mM G
0
10 mV
5s
-80
H
CTL ob/ob
Burst baseline (mV)
**
I
CTL ob/ob
AP baseline (mV)
*
J
CTL ob/ob
Peak (mV)
*

Figure 4.

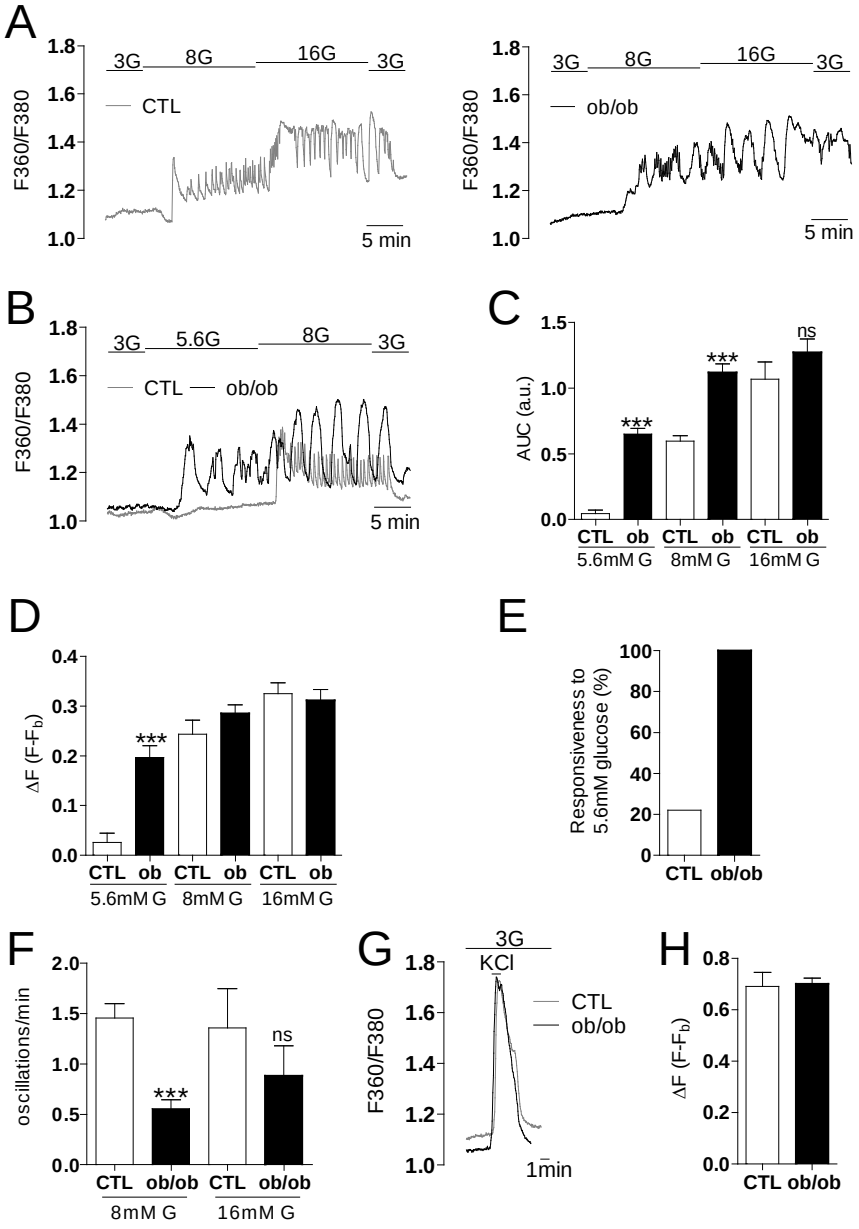
A
3G
8G
16G
3G
CTL
ob/ob
F360/F380
5 min
B
5.6G
CTL
ob/ob
C
AUC (a.u.)
***
ns
CTL
ob
5.6mM G
8mM G
16mM G
D
ΔF (F-Fb)
E
Responsiveness to 5.6mM glucose (%)
CTL
ob/ob
F
oscillations/min
G
KCl
1min
H

Figure 5.

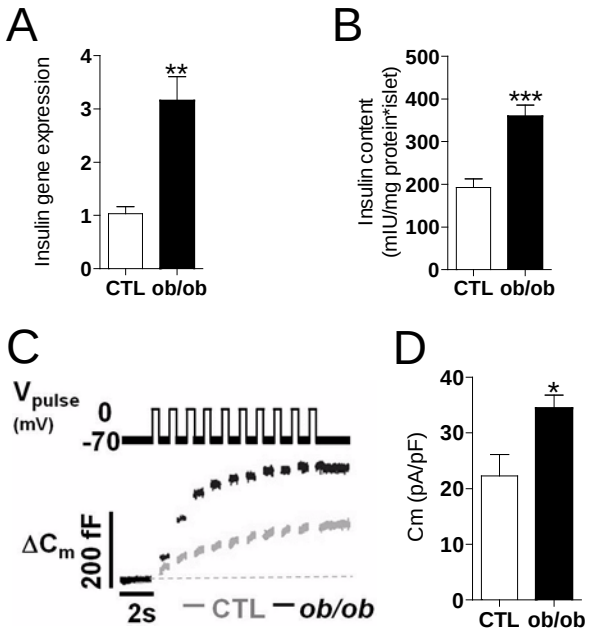
A
Insulin gene expression
4
3
2
1
0
**
CTL ob/ob
B
Insulin content
(mIU/mg protein*islet)
500
400
300
200
100
0
***
CTL ob/ob
C
V pulse
(mV)
0
-70
ΔCm
200 fF
2s
CTL ob/ob
D
Cm (pA/pF)
40
30
20
10
0
*
CTL ob/ob

Figure 6.

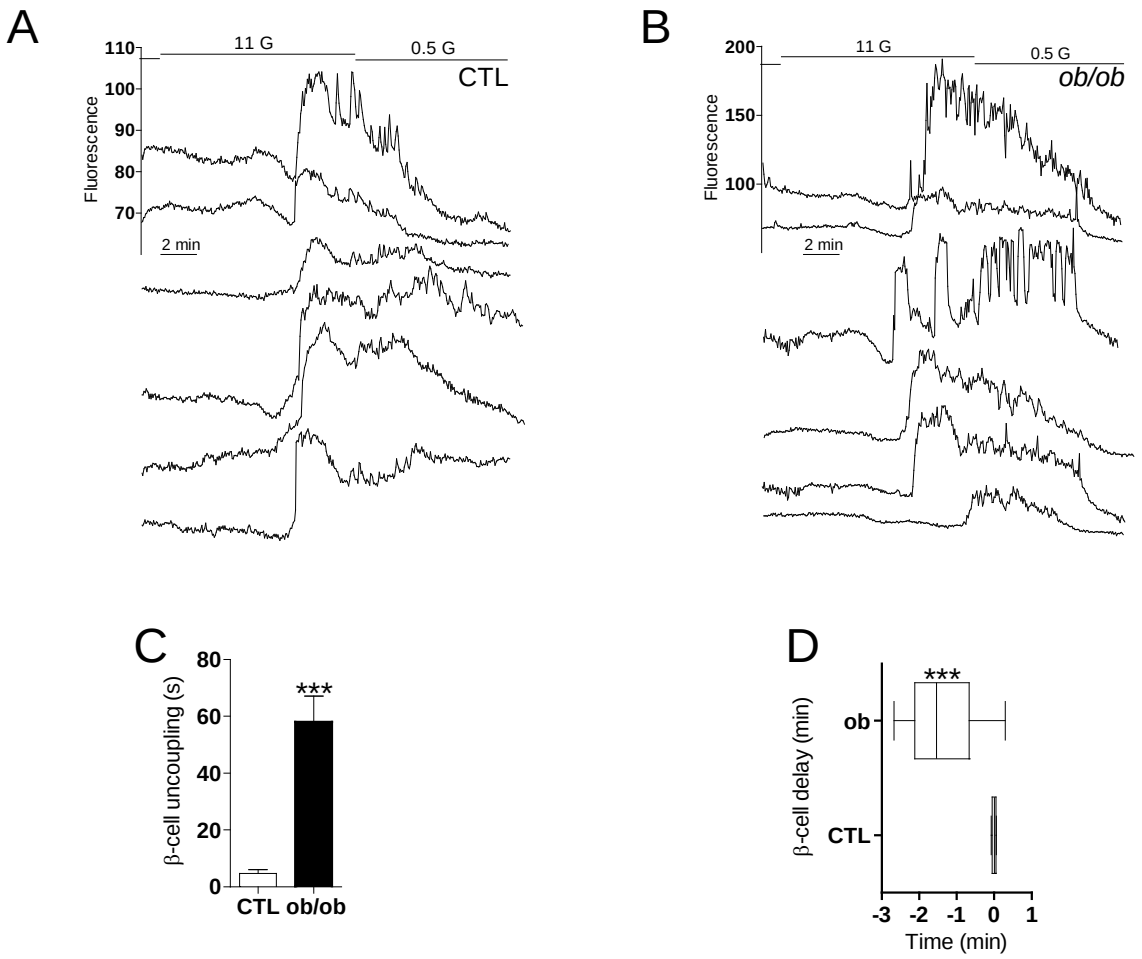
A
11 G
0.5 G
CTL
Fluorescence
110
100
90
80
70
2 min
B
11 G
0.5 G
ob/ob
Fluorescence
200
150
100
2 min
C
β-cell uncoupling (s)
80
60
40
20
0
***
CTL ob/ob
D
***
ob
CTL
β-cell delay (min)
-3 -2 -1 0 1
Time (min)

Supplemental Table 1: Sequences of the primer-pairs used for gene expression analysis.

	Forward 5'-3'	Reverse 5'-3'
GAPDH	CCTGCACCACCAACTGCTTAG	GCCCCACGGCCATCACGCCA
Insulin	AGCAGGAAGGTTATTGTTTC	ACATGGGTGTGTAGAAGAAG
GLUT2	GGAAGAGGCATCGACTGAGCAG	GCCTTCTCCACAAGCAGCACAG
Glucokinase	GAAGCACACTCAGGTCTTGCTC	AAAACAGCCAGGTCTGGGCAGC
Connexin36	ACCATCTTGGAGAGGCTGCTGGA	ATCTTCTCGTTTGCTCCCTCCGC
TRPM5	CAAATCCCTCTGGATGAAATTGATG	CCAGCCAGTTGGCATAGA

Supplemental Figure 1.

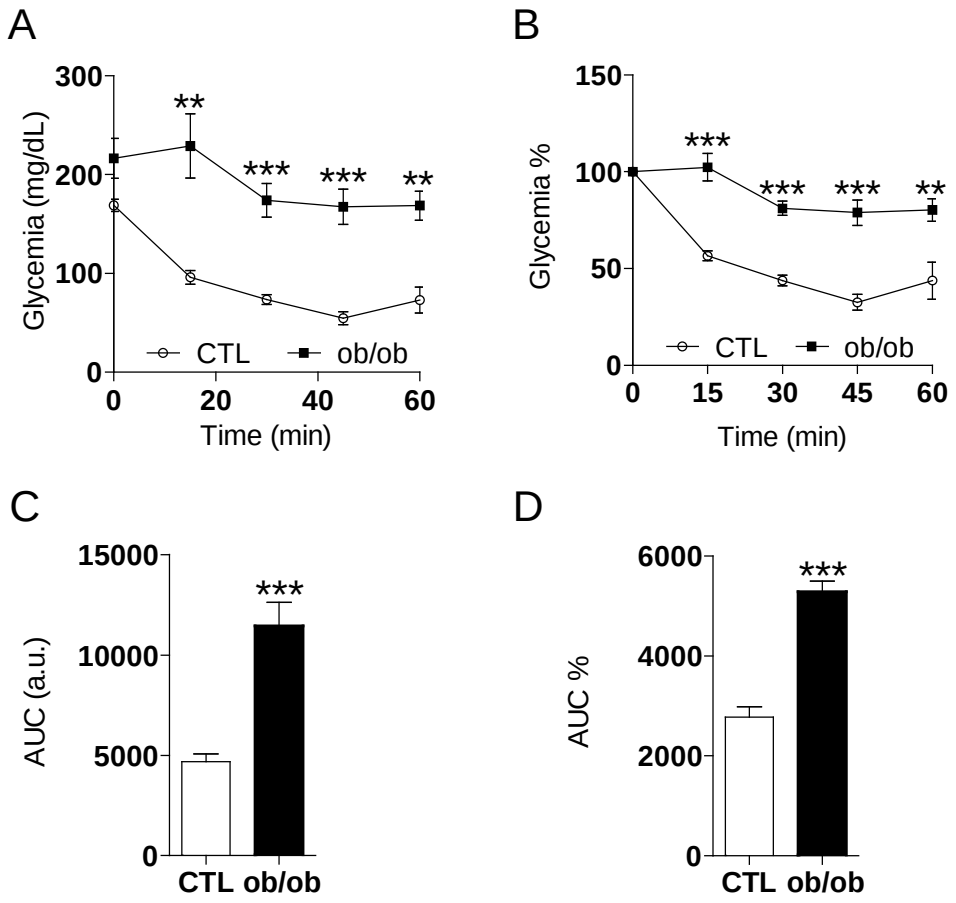

Supplemental Figure 1. Insulin sensitivity. A, Insulin tolerance test in CTL and *ob/ob* mice (n=8 for each group). B, Plasma glucose values during an insulin tolerance test, expressed as the percentage of change of the initial value. C and D, area under the curve of A and B, respectively. E, Plasma glucose before the insulin injection. Statistical significance is indicated: **, $p \leq 0.01$; ***, $p \leq 0.001$;

Supplemental Figure 2.

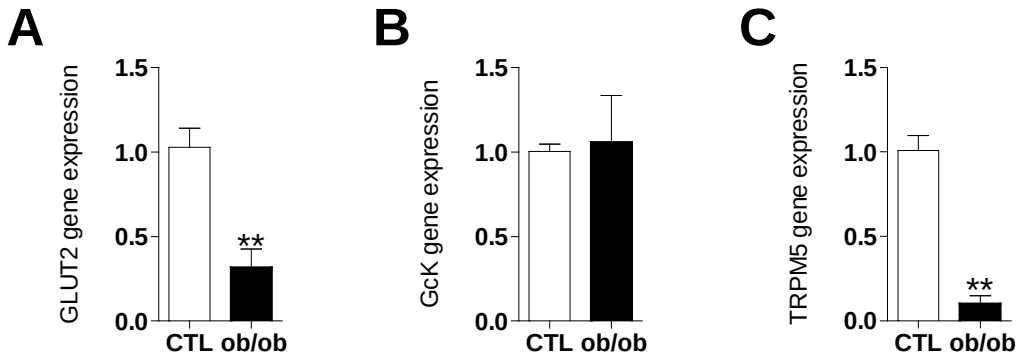

Supplemental Figure 2. Gene expression analysis by qPCR. Relative gene expression of GLUT2 (A), Glucokinase (B) and TRPM5 (C) in islets from CTL and *ob/ob* mice (n=5 for each group). Statistical significance is indicated: **, $p \leq 0.01$

Supplemental Figure 3.

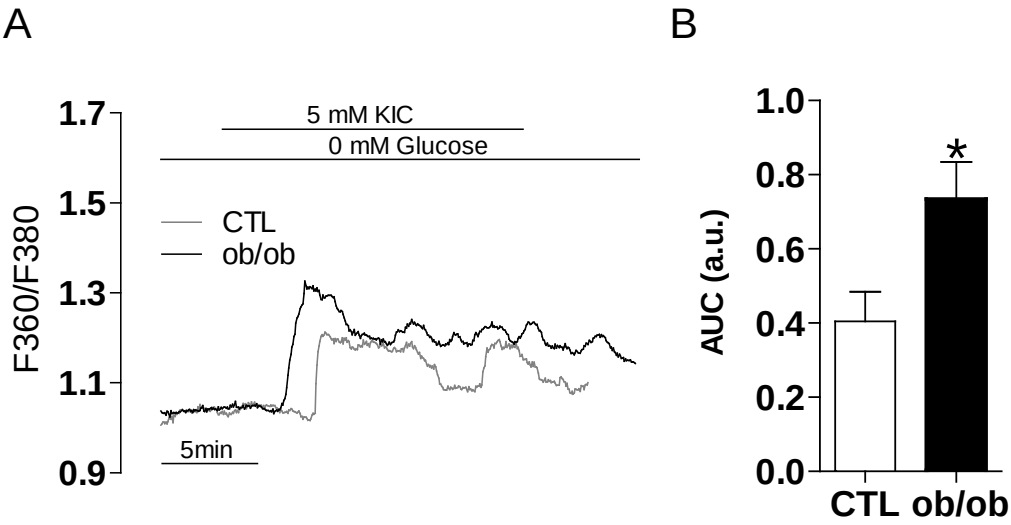

Supplemental Figure 3. Ca^{2+} signaling induced by the non-glucidic fuel α-ketoisocaproate (KIC). A, Representative intracellular Ca^{2+} signals measured in intact CTL and *ob/ob* islets in response to 5 mM KIC (n=6 for each group). B, Area under the curve on the last five minutes of the KIC stimulus from experiment in A. Statistical significance is indicated: *, $p \leq 0.05$.

Supplemental Figure 4.

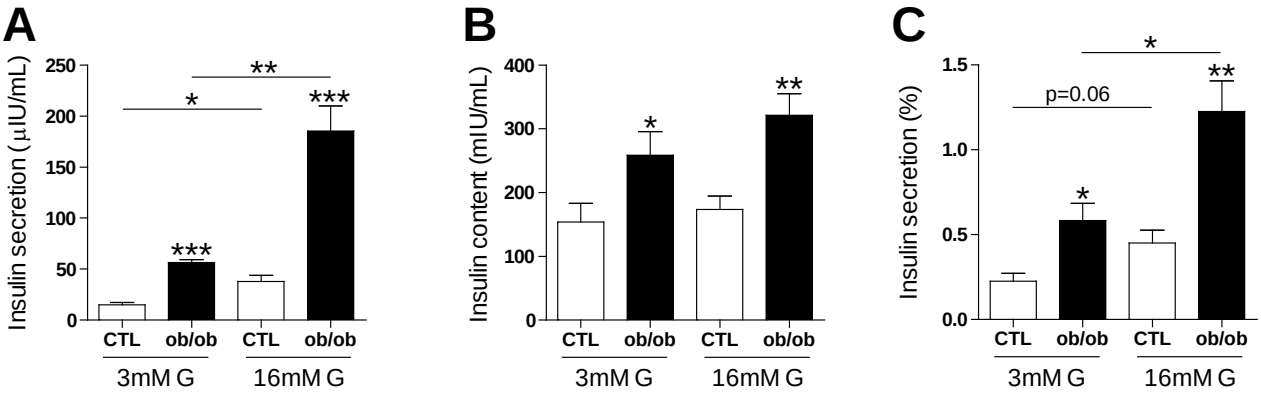

Supplemental Figure 4. *Ex vivo* insulin secretion from CTL and *ob/ob* islets. Insulin secretion (A), insulin content (B) and insulin secretion normalized by insulin content (C) in islets from CTL and ob/ob mice (n=8 for each group). Statistical significance is indicated: *, $p \leq 0.05$; **, $p \leq 0.01$; ***, $p \leq 0.001$; ns, non-significant.

Supplemental Figure 5.

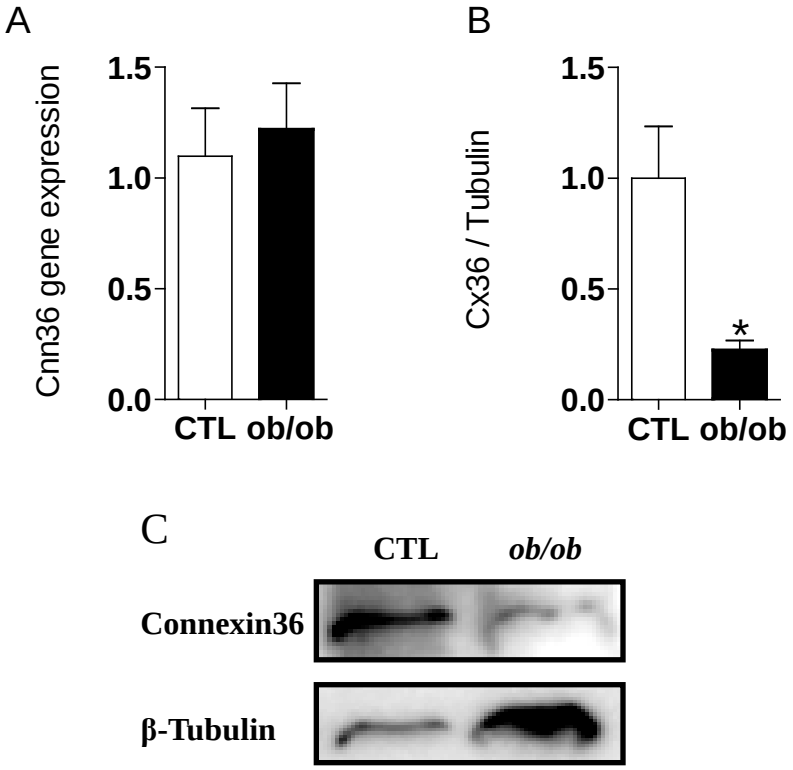

Supplemental Figure 5. Connexin36 expression. A, Connexin36 gene expression in islets of CTL and *ob/ob* mice (n=5 for each group). B, Connexin36 protein expression in islets of CTL (n=4) and *ob/ob* (n=3) mice. C, Representative blots from B. Statistical significance is indicated: *, $p \leq 0.05$.

Supplemental Figure 6.

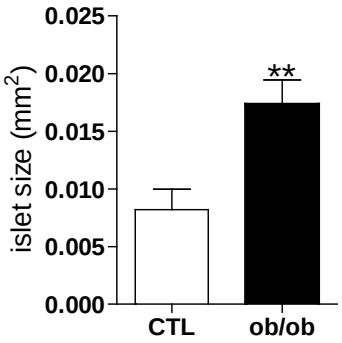

Supplemental Figure 6. Islet size. Thus graph shows the average islet size for CTL (n=316 islets) and *ob/ob* (n=454 islets). Statistical significance is indicated: **, $p \leq 0.01$